Fully Automatic Segmentation of Papillary Muscles in 3-D LGE-MRI

Tanja Kurzendorfer[1], Alexander Brost[2], Christoph Forman[3], Michaela Schmidt[3], Christoph Tillmanns[4], Andreas Maier[1]

[1]Pattern Recognition Lab, Friedrich-Alexander University of Erlangen-Nuremberg, Erlangen, Germany
[2]Siemens Healthcare GmbH, Forchheim, Germany
[3]Siemens Healthcare GmbH, Erlangen, Germany
[4]Diagnostikum Berlin, Kardiologie, Berlin, Germany
tanja.kurzendorfer@fau.de

Abstract. Cardiac resynchronization therapy is a treatment option for patients suffering from symptomatic heart failure. The problem with this treatment option is, that 30 % to 40 % of the patients do not respond. One reason might be the inappropriate placement of the left ventricular lead via the coronary sinus. Therefore, endocardial pacing systems have been developed. Nonetheless, the implantation of these devices requires in addition to the knowledge of the anatomy and scar of the left ventricle (LV), the information of the papillary muscles. As pacing in a papillary muscles may lead to severe problems. To overcome this issue, a fully automatic papillary muscle segmentation in 3-D LGE-MRI is presented. First, the left ventricle is initialized using a registration based approach, afterwards the short axis view of the LV is estimated. In the next step, the blood pool is segmented. Finally, the papillary muscles are extracted using a threshold based approach. The proposed method was evaluated on six 3-D LGE-MRI data sets and were compared to gold standard annotations from clinical experts. This comparison resulted in a Dice coefficient of 0.72.

1 Introduction

Patients suffering from heart failure (HF) may be candidates for implantation of a cardiac-resynchronization-therapy (CRT) device. CRT devices require one lead to be positioned in the coronary vein system for pacing the left ventricle (LV). Nonetheless, about 30 % to 40 % of the patients do not benefit from such a system. There are various issues raised in medical literature. One reason is the confined placement in the venous system [1,2]. To overcome this issue, current research focuses on developing endocardial pacing systems, which allow for free and unrestricted placement of a wireless lead inside the LV. For the implantation of such an endocardial CRT pacing systems, the information about the left ventricle's anatomy, scar and in particular the papillary muscles and the chordae tendineae are highly important. Placing an endocardial lead inside the LV in

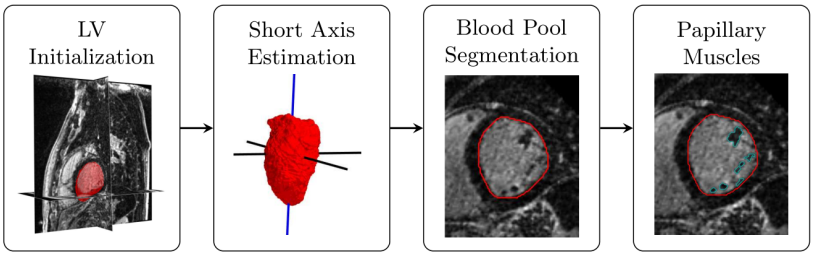

Fig. 1. Overview of the papillary muscles segmentation pipeline. First, the left ventricle is initialized using a registration based approach. In the next step, the short axis view is estimated with the help of principal component analysis. In the third step, the blood pool is segmented in polar space. In the final step, the papillary muscles are extracted using a threshold based approach.

a papillary muscle may lead to complications. However, information about the propagation of papillary muscles is difficult to obtain. In current clinical practice, scar quantification is performed by segmenting the left ventricle in 2-D late gadolinium enhanced (LGE) MRI. Recently, 3-D LGE-MRI acquisitions are developed that allow a full coverage of the entire heart within a single acquisition and a high isotropic resolution [3]. Besides technological improvements regarding image acquisition and the clear clinical demand, the challenge arises in the fast and accurate image analysis. A first semi-automatic solution for myocardial segmentation using solely 3-D LGE-MRI was proposed by Kurzendorfer et al. [4]. In this work, a fully automatic segmentation of the papillary muscles within the left ventricle is presented in 3-D LGE-MRI.

2 Method

The papillary muscles segmentation pipeline consists of four major steps: First, a two-step registration is performed for an initialization of the left ventricle. Second, the principal components of the left ventricle are computed and a pseudo short axis view is estimated. In the third step, the blood pool is segmented in polar space. In the final step, the papillary muscles are segmented using a threshold based approach. Fig. 1 provides an overview of the segmentation pipeline.

2.1 Left Ventricle Initialization

The left ventricle is initialized using a two stage registration [5] with an atlas volume $\mathbf{A} \in \mathbb{R}^{I \times J \times K}$, where I, J and K are the image image dimensions. The segmentation of the atlas volume $\mathbf{A}$ was done manually resulting in a labeled mask $\mathbf{L}$. First, a similarity transform is performed, which allows scaling, rotation and translation. To match the complex deformations of cardiac images a non-rigid registration is applied afterwards. For the matching of the transformation

a mutual information based similarity measure is used [6]. After the registration, the transformation is applied to the atlas label map $\mathbf{L}$ of the atlas volume $\mathbf{A}$, resulting in a registered mask $\mathbf{M} \in \mathbb{R}^{I \times J \times K}$.

2.2 Short Axis Estimation

After the location of the left ventricle is known, the short axis view is estimated using principle component analysis [7]. Therefore, the vertices of the surface of mask $\mathbf{M}$ are extracted using the marching cubes algorithm [8], resulting in $\mathbf{C} \in \mathbb{R}^{N \times 3}$, where N is the number of vertices. Subsequently, the covariance matrix $\mathbf{\Sigma}$ of the contour points is calculated. Having the covariance matrix $\mathbf{\Sigma}$ the singular value decomposition (SVD) is applied, which results in $\mathbf{\Sigma} = \mathbf{USV}^T$, where $\mathbf{U}$ is a 3×3 matrix where the columns are orthogonal unit vectors. The first column corresponds to the largest variation, i.e. the short axis view. The second box of Fig. 1 shows the three unit vectors of $\mathbf{M}$, with the first marked in blue. In the next step, the offset to the center of rotation is calculated. Then, the affine transformation around the unit vectors, considering the offset can be applied to the image volume. The short axis view is needed for the segmentation of the LV, as prior knowledge such as circularity and convexity can be applied.

2.3 Blood Pool Segmentation

As the rough outline of the blood pool is known through the atlas registration, the volume can be cropped to the region of interest. The refinement of the blood pool starts with the slice that corresponds to the center of mass of the contour points $\mathbf{C}$, see Fig. 2 (a) for an example. The polar image of the slice is calculated, where the origin of the polar image corresponds to the center of the found contours, as depicted in Fig. 2 (b). The segmentation is performed in polar space for several reasons: The contours have a roughly circular shape in the short axis view, therefore, in polar space they all have a similar horizontal length. Furthermore, the size of the polar image is smaller, which allows for a faster processing. Through this mapping the Cartesian coordinates (x, y) are converted to polar coordinates (r, ρ). The contours $\mathbf{C}_s$ from the transformed mask $\mathbf{M}$ are converted to polar space, where s corresponds to the current slice index. Fig 2 (c) shows an example of the polar image with the transformed contours. These contours are used to refine the boundaries of the blood pool. For the refinement the edge information is extracted using the Canny edge detector.

To extract minor edges, the standard deviation σ_G of the Gaussian smoothing is set to 2.5, as depicted in Fig. 2 (d). Having the edge image $\mathbf{E}$, a minimal cost path (MCP) search is initialized using six equally spread points from $\mathbf{C}_s$. The MCP finds the distance weighted minimal path through the edge image $\mathbf{E}$. The costs for one move from point $\mathbf{p}_i$ to point $\mathbf{p}_j$ is calculated as follows

$$c(\mathbf{p}_i, \mathbf{p}_j) = \frac{d}{2}\mathbf{E}(\mathbf{p}_i) + \frac{d}{2}\mathbf{E}(\mathbf{p}_j), \tag{1}$$

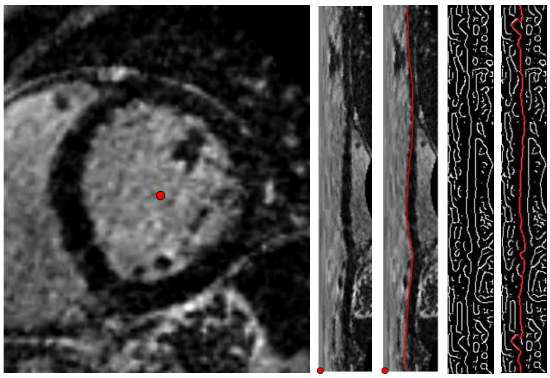

(a) (b) (c) (d) (e)

Fig. 2. (a) Slice in short axis orientation, which corresponds to the center of mass of the mask **M** marked as a red dot. (b) Corresponding image in polar space, where the origin (red dot) corresponds to the center of mass in Cartesian coordinates. (c) Polar image with the transformed contour points $\mathbf{C}_s$ in polar space. (d) Edge information from the Canny edge detector with a Gaussian smoothing of $\sigma = 2.5$. (e) Final result of the MCP.

where $d = ||\mathbf{p}_i - \mathbf{p}_j||_2$. The diagonal moves vs. the axial moves are of different length and therefore, the path costs c are weighted accordingly. The cost path is calculated as the sum of the costs at each point of the path. The result of the MCP is visualized in Fig. 2 (e). The contours from the MCP are converted back to Cartesian coordinates, see Fig. 3 (a). As papillary muscles close to the endocardial border may be included, the convex hull is calculated, as depicted in Fig. 3 (b). After the first contour is refined, these steps are repeated for the subsequent slices in the pseudo SA view until the base and apex are reached. In addition, the information about the shape, radius and center is used to garantee for inter-slice smoothness.

2.4 Papillary Muscles Segmentation

In the next step, the papillary muscles can be segmented. In the first step, morphological erosion is applied to the blood pool contour with a radius of 2 pixels. Afterwards, Otsu thresholding is applied to the blood pool region only. All the pixels that are less than the Otsu threshold θ_O are defined as possible candidates for the papillary muscles. However, if there are not more than 7 pixels connected, it is declared as noise and they are not considered as candidates for the papillary muscles. The final result of the segmented papillary muscles for one slice is visualized in Fig. 3 (c).

After the segmentation is finished, the segmentation mask of the blood pool and the papillary muscles are exported as 3-D surface meshes and can be used for further procedure planning and guidance. See Fig. 3 (d) for an example, with the papillary muscles visualized in blue and the surface of the blood pool in red.

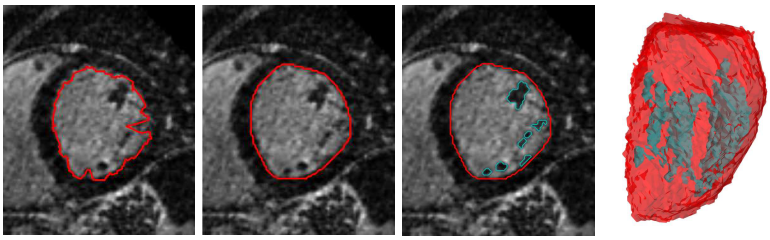

(a) (b) (c) (d)

Fig. 3. Final steps of the segmentation pipeline. (a) Contour points after the MCP in Cartesian coordinates. (b) Convex hull of the MCP, resulting in the final result for the blood pool refinement. (c) Final result showing the blood pool contour in red and the papillary muscles in blue. (d) Result in 3-D, the blood pool is visualized in red and the papillary muscles in blue.

3 Evaluation and Results

The fully automatic segmentation of the papillary muscles was evaluated on six clinical LGE-MRI data sets (sparse GRE prototype sequence and reconstruction, spatial resolution $(1.3\,\mathrm{mm})^3$) from individual patients. The data was acquired with a 3T MAGNETOM Skyra scanner (Siemens Healthcare GmbH, Erlangen, Germany). Gold standard annotations of the papillary muscles were provided by two clinical experts. The annotations were performed using MITK. Given the gold standard annotations, the segmentation was evaluated using the Dice coefficient (DC) and the Jaccard index (JI). The DC is a quantitative measure for the segmentation quality, as it measures the proportion of the true positives in the segmentation. The JI measures the union overlap between two segmentation masks. Both scores range from 0 to 1, with 1 corresponding to perfect overlap. For both scores the whole 3-D volume was considered. The segmentation of the papillary muscles resulted in a DC of 0.72 ± 0.08. The best segmentation result had a DC of 0.85 and the worst a DC of 0.61. For the Jaccard index similar observations could be made, with a mean JI of 0.57 ± 0.10. The best JI had a value of 0.74 and the worst of 0.44.

The evaluation was performed on an Intel i7 with 2.80GHz equipped with 16 GB RAM. The whole segmentation pipeline needs less than 4 minutes implemented with Python, single-threaded.

4 Discussion and Conclusion

The results are summarized in Table 1. The proposed method achieved a DC of 0.72 and a JC of 0.57. The relatively low Dice coefficient can be attributed to the fact, that in one data set the papillary muscles were scarred and sometimes in addition some parts of the chordae tendineae were included in the segmentation.

In sum this work presents a simple and efficient approach for papillary muscle segmentation in 3-D LGE-MRI. The segmented papillary muscles as well as

Description	Mean ± Std	Min	Max	Inter-Obs
Dice	0.72 ± 0.08	0.61	0.85	0.96 ± 0.06
Jaccard	0.57 ± 0.10	0.44	0.74	0.93 ± 0.11

Table 1. Papillary muscles segmentation results using the Dice coefficient and the Jaccard index.

the information about myocardial scarring and the anatomy of the left ventricle can be extracted from one sequence and then be used to plan the procedure. In addition, the papillary muscles can be overlaid onto the fluoroscopic images and used during the intervention for guidance. Future work will include the investigation of scarred myocardium and papillary muscles for further improvement of the segmentation algorithm. A clear benefit of this approach is that all relevant information for a CRT procedure can be extracted from a single LGE-MRI data set.

Disclaimer: The methods and information presented in this paper are based on research and are not commercially available.

References

1. Shetty A, Duckett S, Ginks M, Ma Y, Sohal M, Bostock J, et al. Cardiac magnetic resonance-derived anatomy, scar, and dyssynchrony fused with fluoroscopy to guide LV lead placement in cardiac resynchronization therapy: a comparison with acute haemodynamic measures and echocardiographic reverse remodelling. Eur Heart J Cardiovasc Imaging. 2012 November;14(7):692–699.
2. Shetty A, Sohal M, Chen Z, Ginks M, Bostock J, Amraoui S, et al. A comparison of left ventricular endocardial, multisite, and multipolar epicardial cardiac resynchronization: an acute haemodynamic and electroanatomical study. Europace. 2014 February; p. eut420.
3. Shin T, Lustig M, Nishimura D, Hu B. Rapid single-breath-hold 3D late gadolinium enhancement cardiac MRI using a stack-of-spirals acquisition. J Magn Reson Imaging. 2014 December;40(6):1496–1502.
4. Kurzendorfer T, Brost A, Forman C, Schmidt M, Tillmanns C, Hornegger J. Semi-Automatic Segmentation and Scar Quantification of the Left Ventricle in 3-D Late Gadolinium Enhanced MRI. In: ESMRMB, editor. 32nd Annual Scientific Meeting of the ESMRMB; 2015. p. 318–319.
5. Unberath M, Maier A, Fleischmann D, Hornegger J, Fahrig R. Comparative Evaluation of Two Registration-based Segmentation Algorithms: Application to Whole Heart Segmentation in CT. In: Leonhardt S, editor. Proceedings of the GRC; 2015. p. 5–8.
6. Klein S, Staring M, Murphy K, Viergever MA, Pluim JP. elastix: A Toolbox for Intensity-Based Medical Image Registration. IEEE Trans Med Imaging. 2010 January;29(1):196–205.
7. Jolliffe I. Principal Component Analysis. Wiley Online Library; 2002.
8. Lorensen W, Cline H. Marching Cubes: A High Resolution 3D Surface Construction Algorithm. In: ACM Siggraph Computer Graphics. vol. 21. ACM; 1987. p. 163–169.